JGR Space Physics

RESEARCH ARTICLE
10.1029/2018JA025692

Spatial Gradients in Geomagnetic Storm Time Currents Observed by Swarm Multispacecraft Mission

Geeta Vichare[1], Neethal Thomas[1,2], Kazau Shiokawa[2], Ankush Bhaskar[1,3], and Ashwini Kumar Sinha[1]

[1]Indian Institute of Geomagnetism, Navi Mumbai, India, [2]Institute for Space-Earth Environmental Research, Nagoya University, Nagoya, Japan, [3]NASA Goddard Space Flight Centre, Greenbelt, MD, USA

Key Points:
- Geomagnetic storm time magnetic field variations are stronger in the dusk-night than the dawn-day sector
- Longitudinal gradients in the storm time magnetic field are stronger near the equator and support the idea of particle injection from tail
- During episodes of substorm, stronger longitudinal gradients are observed at higher latitudes (~40°), which might be associated with FACs

Correspondence to:
G. Vichare,
vicharegeeta@gmail.com

Citation:
Vichare, G., Thomas, N., Shiokawa, K., Bhaskar, A., & Sinha, A. K. (2019). Spatial gradients in geomagnetic storm time currents observed by Swarm multispacecraft mission. *Journal of Geophysical Research: Space Physics*, *124*, 982–995. https://doi.org/10.1029/2018JA025692

Received 18 MAY 2018
Accepted 6 JAN 2019
Accepted article online 15 JAN 2019
Published online 9 FEB 2019

Abstract This paper presents a comprehensive study of geomagnetic storm time currents using magnetic field recorded by multispacecraft polar-orbiting mission, Swarm. During geomagnetic storm period, the magnetic field variations obtained after removing the internal geomagnetic field and quiet time contributions can be considered as a proxy for storm time currents and are found to follow the temporal profile of Dst index very closely. These variations at the equatorial crossings recorded by multiple-spacecraft are used to estimate the Dst values and are found to have a good match with the ground-based Dst index. The average deviation between these two is around 4–13%. We have estimated the asymmetry by taking the difference between the magnetic field variations at two local time sectors separated by 12 hr. The estimated asymmetry shows a good match with the AsyH-index, especially when satellite traverses in the dawn-dusk sector. In general, the magnetic field variations are stronger in the night-to-dusk sector than day-to-dawn sector, which could be due to the larger pressure-gradients near night-to-dusk caused by ion movements. The important advantage of Swarm mission is that it provides an opportunity to investigate the longitudinal gradients in the storm time magnetic fields. It is observed that in general, the gradients are stronger during the main phase of the storm, centered near the equator with a latitudinal width of ~20–30° in both the hemispheres, and are supportive to the scenario of particle-injection from the magnetotail. The stronger gradients are observed at higher latitudes (~40°) during the episodes of substorms and might be associated with the ionospheric/field-aligned currents.

Plain Language Summary The space weather events such as geomagnetic storms can have a huge impact on the terrestrial magnetic and plasma environment, producing large currents, which in turn, impact spaceborne communication, navigation systems, aviation and satellite operations, and electric power grids, etc. The paper presents a new approach to estimate geomagnetic indices equivalent to Dst and AsyH during geomagnetic storms, making use of the increased observations from space-based instruments in recent times, and demonstrates their utility in quantifying the geomagnetic environment. The important advantage of multispacecraft Swarm mission is that it provides an opportunity to investigate the spatial gradients in the storm time magnetic fields. The paper reports that strong azimuthal gradients in the magnetic field, near the equatorial sector, are associated with particle injection from the magnetotail. The paper demonstrates the utility of space-based measurements in understanding the geomagnetic environment.

1. Introduction

Geomagnetic storms are produced by enhanced solar wind-magnetosphere energy coupling through the mechanism of magnetic reconnection (Dungey, 1961). A typical geomagnetic storm signature is characterized by a depression in the horizontal component of the geomagnetic field at low to middle latitudes, which is due to the ring current encircling around the Earth in a westward direction in the equatorial plane and can be monitored by the Dst or SymH index (Daglis et al., 1999; Kamide et al., 1997). The asymmetric part of the ring current is indicated by AsyH index. These indices are computed using the magnetic field measurements at longitudinally separated low latitude ground stations (details at http://wdc.kugi.kyoto-u.ac.jp).

Geomagnetic storms have been explored extensively from the ground as well as spaceborne platforms (Abdu et al., 2006; Dunlop et al., 1988; Horvath & Lovell, 2014; Liemohn et al., 2001; Munsami, 2000; Rangarajan, 1989; Sugiura, 1964; Weygand & McPherron, 2006). It has been realized that the presence of field-aligned

currents (FACs), ionospheric closure currents, substorm current wedge, magnetopause currents, magnetotail currents, prompt penetration electric fields, etc., during storm time can cause asymmetry in the ring current (Akasofu & Chapman, 1964; Dubyagin et al., 2014; Friedrich et al., 1999; Greenspan & Hamilton, 2000; Liemohn et al., 2001; Siscoe & Crooker, 1974; Turner et al., 2000). Using magnetic field measurements from magnetospheric four-satellite mission, Cluster, as well as from various polar low Earth orbiting (LEO) satellites, the storm time FACs have been estimated using Ampere's law (Dunlop et al., 2002; Lühr et al., 1994, 2015; Robert et al., 1998). Also, attempts have been made using polar LEO satellite such as CHAMP to investigate the effects of geomagnetic storms on thermosphere/ionosphere system (Balan et al., 2012; Manoj et al., 2013; Oliveira et al., 2017). These studies are mainly based on the electron density measurements and wind drag information derived from LEO observations. Balasis et al. (2012) have studied the ultralow frequency wave activity during geomagnetic storm using multipoint observations from CHAMP, Cluster, and Geotail missions. Recently, Swarm satellite measurements are used for studying geomagnetic storms (Astafyeva et al., 2016; De Michelis et al., 2016). De Michelis et al. (2016) analyzed the dynamical changes in the magnetic field scaling features during the development of the geomagnetic storm. Astafyeva et al. (2016) investigated the storm time evolution of the ionospheric response. Dunlop et al. (2015) reported matching signatures of FACs simultaneously near the ionosphere at Swarm orbit (~500 km) and in the magnetosphere (Cluster satellites). Hamilton (2013) presented a scheme to study the magnetospheric and corresponding induced fields through Fast Track Magnetospheric Model (FTMM) using LEO satellites.

It is known that temporal changes in the baseline of Dst index hurdle the geomagnetic field modeling. Therefore, Olsen et al. (2014) derived a new index called *RC index*, which describes the strength of the background ring current present even during geomagnetic quiet conditions. It is derived by an hour-by-hour spherical harmonic analysis of hourly values of the magnetic field from ground geomagnetic observatories located at middle to low latitudes and nighttime sector. National Aeronautics and Space Administration (NASA)'s Van Allen Storm Probes have made direct measurements of the ring current particle population and deduced the ring current intensity (Lanzerotti & Gerrard, 2016). Another NASA mission of Image satellite carried the Energetic Neutral Atom imagers from which the ring current intensity was inferred (Brandt et al., 2002). Applying curlometer technique to the magnetic field observed by Cluster spacecraft, Zhang et al. (2011) deduced the azimuthal distribution of ring current. Thus, there are attempts to estimate ring current either through direct or indirect measurements.

The purpose of the present paper is to investigate storm time currents using multipoint magnetic field measurements from the Swarm satellite constellation. Swarm mission satellites A and C orbit side by side at an altitude of ~470 km, and satellite B orbits at an altitude of ~520 km above the Earth's surface. As the mission progresses, satellite B moves away from the other two satellites in longitude. The separation was of ~ 30° during April 2014 to August 2015. Here we present a method to compute Dst index using multipoint spaceborne measurements. The method of data analysis and observations are described in section 2. Sections 3 and 4 sketch the scheme to estimate symmetric and asymmetric part of the storm time ring current, respectively. We have compared our estimates with the actual Dst index for the geomagnetic storms occurred during April 2014 to August 2015. We believe that this is the first explicit study on the storm time current using polar orbiting LEO satellite magnetic field observations. Longitudinal gradients in the storm time currents are investigated in section 5. Finally, sections 6 and 7 discuss and summarize the results.

2. Data Analysis and Observations

We analyze magnetic field data of 1-Hz resolution recorded by European Space Agency's Swarm mission satellites (Friis-Christensen et al., 2006; Olsen et al., 2013). To remove the contribution from the internal origin, we used Chaos model (CHAOS-6) of geomagnetic field (Olsen et al., 2016), which is subtracted from the satellite observations. Note that we subtracted only the main and crustal field components and did not remove any external contribution or induced current component. In order to remove quiet time ionospheric current contribution such as equatorial electrojet, Sq, from the Swarm magnetic field measurements, we selected nearby geomagnetic quiet day and subtracted the residual magnetic field of quiet time passes having similar longitude (±10°) and nearly same local time (LT; within ±0.5 hr). This removes the contribution due to quiet time currents to some extent and also regional anomalies present, if any. Figure 1 shows the latitudinal profile of the residual field variations (obtained after removing main field model) in the total magnetic

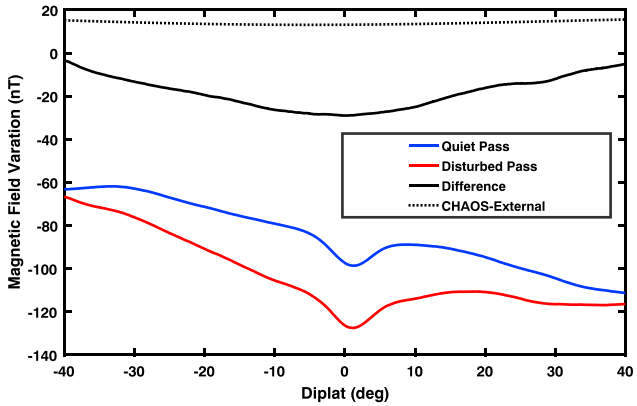

Figure 1. Magnetic field (total component) variations at the topside of the ionosphere after subtracting the internal geomagnetic field. The blue curve is during a typical geomagnetic quiet time conditions (24 December 2013—satellite A; longitude: 339°E; local time: 12:03), the red curve is during geomagnetic storm (25 December 2013—satellite A; longitude: 342 E; local time: 11:58), and the black curve is obtained after subtracting quiet time variations from storm time. The black dashed curve is the ring current contribution from CHAOS model.

field (ΔF). The red curve shows typical daytime satellite pass during geomagnetic storm on 25 December 2013, and the blue curve is that during geomagnetic quiet conditions on 24 December 2013 ($\sum Kp = 3-$). The displayed storm time Swarm A satellite pass traversed over the longitude of 342°E, with near noon LT. The quiet time pass selected for the subtraction was also in the near noon LT sector with a longitude of 339°E. The variations within ±40° geomagnetic latitude are shown here. Both these curves show the presence of daytime equatorial electrojet near the equator (strong dip in the equatorial belt within ±10° latitude). The details of the equatorial electrojet signatures in LEO satellite observations can be found in Jadhav et al. (2002a, 2002b) and Thomas et al. (2017). In order to remove the quiet time ionospheric current contribution from the disturbed time profile, we subtracted the blue curve from the red one. The resultant profile (black curve) obtained after removing the quiet time ionospheric contribution shows broad variations in latitude without equatorial electrojet signature. This variation essentially represents the variations due to storm time currents such as symmetric ring current, partial ring current, magnetopause currents, field aligned currents, and magnetotail currents. The negative variation, which is stronger near the equator, may indicate magnetospheric westward current encircling in the equatorial plane around the Earth. Thus, the broad latitudinal variation may be considered as a proxy of ring current variation. Here dashed curve indicates the external field contribution obtained from CHAOS model considering RC index (Olsen et al., 2014). Note that the external field estimated by CHAOS is too weak compared to the magnetospheric currents estimated through present analysis.

2.1. Geomagnetic Storm on 8 June 2015

Figure 2 shows the latitudinal profile of the storm time fields (residual fields in total component) during each pass of Sat A, on 8 June 2015, when a geomagnetic storm (SymH ~ −105 nT) occurred. Here onward, we will refer *residual fields* as the magnetic field variations obtained after removing the geomagnetic field and quiet time current contributions. Figures 2a and 2b show the latitudinal profiles of residual magnetic field variations during daytime and nighttime passes, respectively. SymH and AsyH indices are plotted in Figure 2c. The onset of the storm took place at ~6 UT, and the main phase continued till ~8 UT, followed by the recovery. But again at ~12 UT, the SymH index started decreasing. This second decrease in SymH may indicate the intensification of the ring current or could be associated with substorm activity or decrease in the solar wind pressure. From the online SuperMAG service portal, it is found that the feature is seen at all local times and hence not due to the substorm phenomenon. So this decrease could be associated with the drop in the solar wind pressure (Figure 7) or due to the strengthening of the ring current. We have divided the storm period into three parts, viz., (i) prestorm phase, (ii) main and early recovery phase, and (iii) late recovery phase. We have shaded these regions with different background colors in Figure 2c.

Note that during the event, Sat A traversed in near noon-midnight orbit (Table 1). The stack plots in Figures 2a and 2b are arranged with increasing UT from bottom to top, and for this reason, an additional vertical shift is introduced in the depicted profiles. Here we wish to show how the latitudinal profiles of different passes change, as the storm progresses. The UT indicated by the right end of the pass is the time (UT) of the equatorial crossing during that satellite pass. Being a polar orbiting mission, Swarm satellites cover the entire latitudinal range in about 45 min during its half orbit. For the convenience of the reader, we have used different colors for the passes corresponding to above mentioned three parts of the storm. Passes before the commencement of the storm (0–6 UT) are shown by green color (prestorm phase). Satellite passes during main and early recovery phase between 6 UT to 16 UT are shown by red color (main and early recovery phase), and those during late recovery phase are shown by blue color.

One can observe that the latitudinal profiles of the residual fields before the onset of the storm (green curves) are almost flat during nighttime, and small variation is observed during daytime passes. The bottommost plot during daytime shows little dip near the equator, but the second plot from the bottom, which is at ~2:30 UT, shows increase near the equator, which could be associated with some positive undulations

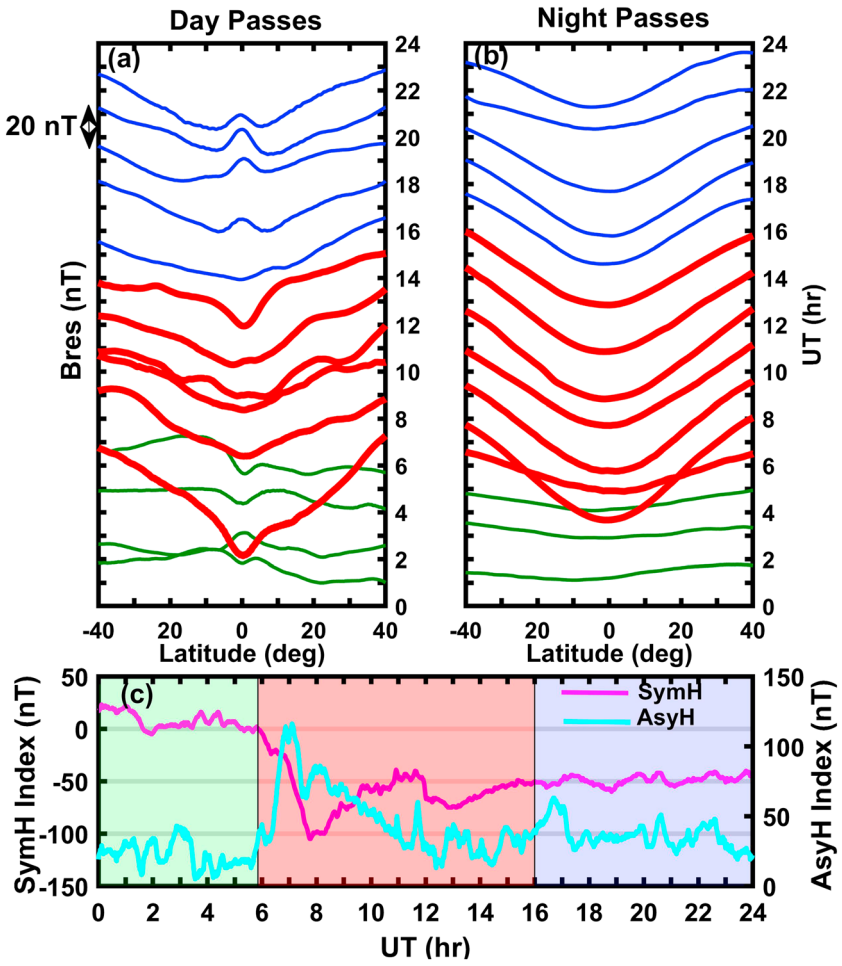

Figure 2. (a and b) Stack plots of residual fields, that is, the latitudinal profiles of the total magnetic fields due to storm time currents at different passes of satellite A on 8 June 2015, during the day (local time ~12:15) and night (local time ~00:15) times, respectively. UTs of equatorial crossings of satellite passes are indicated by the right most end of the pass on the *y* axis shown on the right side of the panels. The green, red, and blue color plots indicate the passes during prestorm, main-early recovery, and late recovery phases respectively. (c) SymH and AsyH variations. SymH scales marked on the left axis and AsyH on the right axis.

observed in the SymH before the onset of the storm. Also, in the recovery phase at 1900, 2030, and 2200 UT, similar pattern of increased variations near the equator is observed.

During the main and early recovery phase of the storm, the residual fields at the night as well as day time passes show large negative variations, peaking near the equator (red color plots). The amplitude of the variation reduces in the recovery phase (blue curves). The latitudinal profiles of the variations are quite smooth in the night sector, whereas dayside profiles show additional modulations over the broad trend. Sometimes, signatures similar to equatorial electrojet appear in the residuals (e.g., residuals at 0700, 1500 UT), which could be due to prompt penetration of storm time electric fields. And the signatures similar to counter electrojet (Vichare & Rajaram, 2011) between 18 and 23 UT could be due to the dominance of the overshielding fields during the late recovery phase.

2.2. Geomagnetic Storm on 17–18 March 2015

The most intense geomagnetic storm of solar cycle 24 till date took place during 17–18 March 2015. The SymH index reached below ~ −200 nT. During the period of this storm, Swarm-A satellite traversed in the early morning (~07:30 LT) and evening local times (~19:30 LT), whilst satellite B revolved in 09–21 LT sector. We have considered here only satellites A and B, as satellites A and C fly almost in the same LT sector.

Table 1
List of Geomagnetic Storms

Sr. no	Event	LT range		Minimum SymH
		Satellite A	Satellite B	
1	8 December 13	0130–1330	0130–1330	−72
2	25 December 13	1130–2330	1130–2330	−45
3	18 February 14	0630–1830	0630–1830	−127
4	17 March 15	0730–1930	0900–2100	−234
5	8 June 15	0015–1215	0215–1415	−105
6	22 June 15	1100–2300	0100–1300	−139
7	15 August 15	0600–1800	0815–2015	−75
8	23 August 15	0500–1700	0730–1930	−62

The magnetic fields of quiet time (22 March 2015) passes in the nearby longitudes (within ±10°) and local times (within ±30 min) are subtracted from the storm time passes. We have plotted this difference (which can be considered to represent the variations due to storm time currents) during different satellite passes in the course of geomagnetic storm on 17–18 March 2015 in Figure 3. The residuals along the passes (within ±40° geomagnetic latitude) of satellites A and B are shown in the upper panel. Note that satellite A has alternate passes near dawn (7:30 LT) and dusk (19:30 LT) sectors, while satellite B has alternate day (9 LT) and night (21 LT) passes. The red and black colors indicate near dawn/day and dusk/night satellite passes, respectively. These residuals are compared with SymH index, which is shown by magenta color. The vertical dashed lines indicate the times of equatorial crossings by satellites A and B. AsyH index is shown in the bottom panel. Note that in the upper panel we are showing the results from two satellites, and hence, there are two vertical dashed lines, indicating the times of equatorial crossings by satellites A (blue) and B (orange). We have extended these dashed lines though out the upper panel so that the spacing between these lines would give an idea about how the timings of the equatorial crossings by two satellites (A and B) deviate from each other. It can be noticed that the spacing between these lines varies with time and is not constant, making the lines sometimes to overlap on each other, or sometimes well separated. For example, up to 12 UT on 17 March, the timings of equatorial crossings for satellites A and B are well separated (~30 min difference), but at 21 UT the difference is small up to 5–10 min. At 8 UT on 18 March the equatorial crossings by satellites A and B occur almost simultaneously.

The St. Patrick's Day storm on 17–18 March 2015 composed of storm sudden commencement (SSC), initial, main, and recovery phases. The sudden impulse of ~50 nT magnitude occurred at ~5 UT on 17 March. The SymH index dropped by ~ −100 nT at ~9 UT and then started recovering, but soon later again started decreasing. SymH reached ~ −200 nT at ~23 UT; thus, the main phase of the storm showed two-step decrease with total main phase interval of ~17 hr. Then the recovery took place during almost entire day on 18 March. Interestingly, the satellite data show the trend similar to SymH, including the double step of

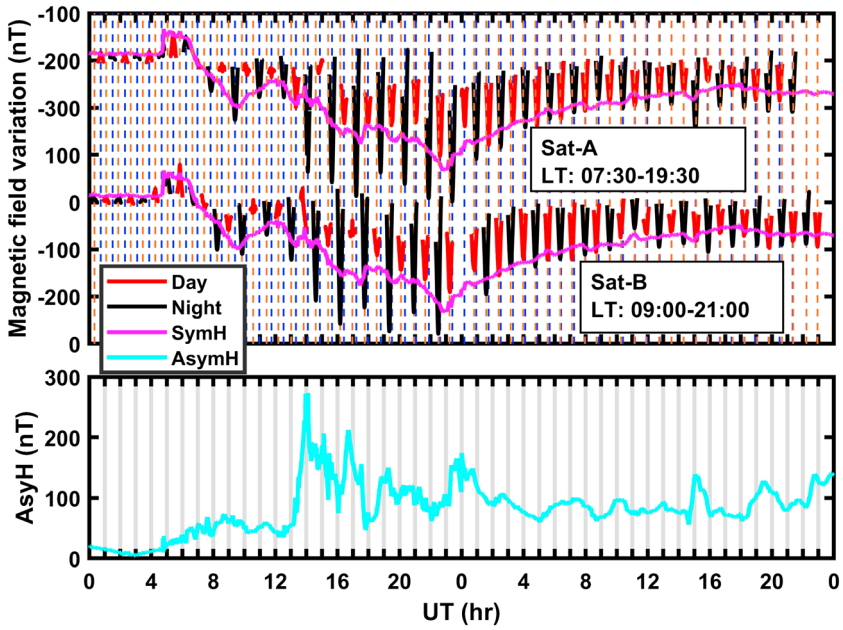

Figure 3. Upper panel shows temporal variations in the magnetic field profiles due to storm time currents, as seen by satellites A and B during geomagnetic storm on 17–18 March 2015, dawn/daytime (red) and dusk/nighttime (black) passes, along with SymH index (magenta). The vertical dashed lines in the upper panel indicate the times of equatorial crossings by satellites A (blue) and B (orange). The bottom panel shows the AsyH index, during the event.

the main phase. The residual fields are very small before the SSC, indicating the absence of any significant currents. At the time of SSC, the satellite fields exhibited *inverted V* type signature, indicating an increase in the magnetic field value, which maximizes near the equator. The variation in the residual profiles increases as the storm main phase progresses and then decreases in the recovery phase of the storm (Figure 3). Note that not only the variation within ±40° enhances, but the entire latitudinal profile moves toward stronger negative values from the prestorm level. The variations during multisteps in the main phase are also marked by the satellite measurements. Thus, the temporal variations in SymH index and satellite-based magnetic field values match very well.

Moreover, one can notice that there is a discernible difference between the amplitudes of the magnetic field variations during morning/near-dawn and night/near-dusk passes, with stronger amplitudes during night/near-dusk time passes. The difference between day and night passes becomes large especially during the main phase of the storm. Interestingly, the AsyH index also shows enhanced values during that time. Since AsyH index essentially gives the asymmetry seen at different local time sectors, the day (dawn)-night (dusk) asymmetry recorded by the satellite can be related to the AsyH index.

3. Computation of Dst Index

As discussed in the previous section, the residual fields can be considered as a proxy of storm time magnetospheric currents. Within a time interval of about 1 hr, each satellite crosses the equator twice (half orbital period is ~45 min). We utilize the measurements at the equatorial crossings by satellites A and B to estimate the Dst index, which is computed by taking an average of the measurements at these equatorial crossing points. One can notice from Figure 3 (vertical dashed lines) that the equatorial crossing times of satellites A and B can be nearly simultaneous or may differ by ~ 25 min. We have selected a window of 2 hr and collected all the available equatorial crossing points of satellites A and B. This ensures the availability of at least four points. Average of these points is considered as an estimate of Dst index. This procedure is repeated by sliding the window by 1 hr. Thus, we get the estimate of Dst values at each hour.

The temporal profiles of Dst estimates based on Swarm satellite measurements are compared with the ground-based Dst and SymH indices during five geomagnetic storms occurred between April 2014 and August 2015, listed in Table 1 (Sr. No. 4–8) and are shown in Figure 4a. The Dst values are not estimated for the first three storms, which took place during the early phase of the Swarm mission, when satellites A and B were placed very close in longitudes. It can be noted that in general, the match of our estimates is very good with the Dst index. It is observed that sometimes the present Dst estimates as well as ground based Dst values deviate from SymH index, which could be due to the resolution differences. The percentage deviations of present Dst estimates from standard ground-based Dst index with respect to the minimum value of Dst index are depicted in Figure 4b. The deviations are in general less than 20%, indicating a good match of our estimates with ground-based Dst index. During the event of 15 August 2015, the deviation appears larger (>50%) near 13 UT. However, one can notice that the match of our estimates with SymH index is better compared to that with Dst index (Figure 4a). Note that in the present study, the Dst is estimated by taking average of the equatorial magnetic field values observed by satellites A and B over 2-hr time window. With an orbital period of ~90 min, each satellite will cross the equator 2–3 times within the duration of 2 hr, providing up to 4 to 6 observations by the two satellites. Thus, we have estimated Dst by averaging these 4–6 values, which are recorded at different UTs within the specified time window of 2 hr. Standard ground-based Dst estimates are based on the hourly averaged values (60 min average) at different ground observatories. Therefore, the finer structures that are present in the SymH index (1-min resolution) will be averaged out in the ground-based Dst index, whereas our Dst estimates sometimes show up these finer structures, and hence sometimes match better with SymH rather than Dst index. The average percentage of deviation of our estimates from the standard Dst index for each storm varies from 4 to 13%.

4. Asymmetry in the Storm Time Current

As noted in Figure 3, the magnetic field values vary considerably between day/dawn and night/dusk passes, thereby indicating azimuthally asymmetric part of the storm time current. Unlike the standard method of estimating AsyH index (subtracting the symmetric ring current contribution from each station and then taking the maximum range of variation), we estimate the asymmetry directly by taking the difference between

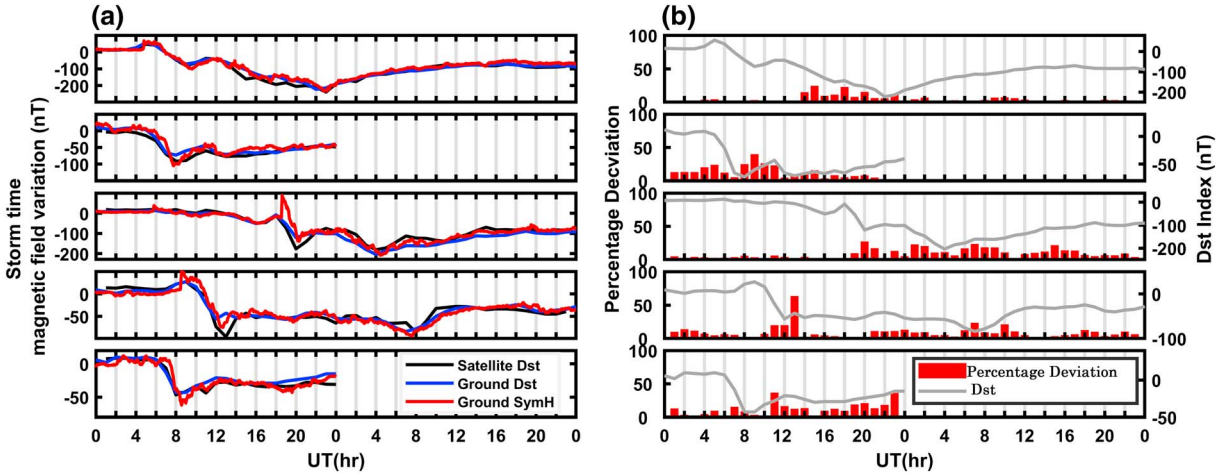

Figure 4. (a) Comparison between Dst index estimated using satellite (black curve) and ground (blue) observations, and SymH index (red). (b) Percentage deviation of satellite-based estimates of Dst from ground-based Dst index.

day/dawn and night/dusk passes. The asymmetry (difference between day/dawn and night/dusk sectors) using satellites A and B is estimated separately. The deviations of the asymmetry derived by the satellite passes from the AsyH index are normalized with respect to the maximum value of the AsyH index. Figures 5a and 5b display the percentage deviation of the asymmetry seen by the satellites A and B, respectively. The AsyH index itself is plotted in the background (grey curve). The deviations when satellite orbits in the dawn-dusk sector are shown by blue color, and other LT sectors are shown by red color. One can notice that the deviation is in general less (<50%) when the satellite traversed in the dawn-dusk sector. The average % deviation in different time sectors is shown in Figure 6. It can be noticed that the average deviation is ~24% when satellite traverses near the noon-midnight meridian are considered. The deviation drops significantly to ~8% when the satellite passes in near the dawn-dusk meridian. The blue curve shows the average pattern along with the standard error bars, computed for 2-hourly bin with an overlap window of 1 hr. This indicates that the asymmetry observed by AsyH index is better represented by the difference between dawn-dusk sectors. Thus, the present analysis demonstrates that the major source for the observed asymmetry lies in the dawn-dusk sector.

5. Longitudinal Gradients

Satellites A and C orbit in the nearby longitudes with very small separation (difference < 2°) and can be used to compute the longitudinal gradients. Thus, Swarm gives unique opportunity to examine how the longitudinal gradients of the magnetic field during disturbed time differ in different magnetic local time (MLT) sectors and whether these gradients vary with latitude. In section 2, we have derived the time profile of the storm time current (residual field after subtracting main and quiet time ionospheric current contribution). The temporal profile of the values of the residual fields (Figure 3) at a particular latitude (e.g., values at the equator are used for Dst estimates) is obtained using satellites A and C separately. It should also be noted that the latitudinal difference between satellites A and C is ~0.5°, and hence, for a particular latitude, the time (UT) differs only by ~7–8 s in both the profiles (satellites A and C), and thus, the gradients due to temporal changes are very small. Although, the longitudinal gradients at particular latitude are estimated by eliminating the time difference through interpolation.

The longitudinal gradient at a fixed latitude is computed as follows

$$\text{Longitudinal Gradient}\ (\theta) = \frac{\text{Res B}_{\text{Sat A}}(\theta) - \text{Res B}_{\text{Sat C}}(\theta)}{\phi_{\text{Sat A}}(\theta) - \phi_{\text{Sat C}}(\theta)} \quad (1)$$

where $\text{Res B}_{\text{Sat A}}(\theta)$ and $\text{Res B}_{\text{Sat C}}(\theta)$ represent the residual magnetic field at a given latitude θ, using satellites A and C, respectively. ϕ is the longitude.

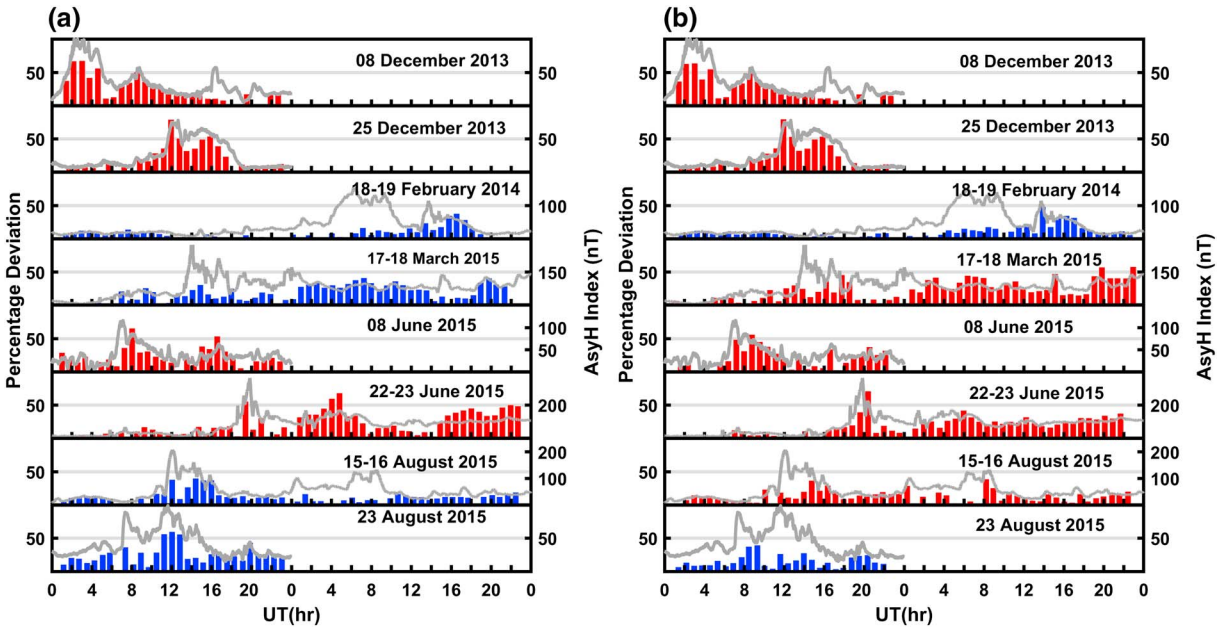

Figure 5. Percentage deviations of the asymmetry from AsyH index, seen by satellites (a) A and (b) B, shown by bar plots. The blue color bars are used when satellite traverses in the dawn-dusk sector; otherwise, the red color bars are used. AsyH index is shown by grey color.

The contour plots of these gradients in UT-latitude frame, in day and night sectors, during geomagnetic storm on 8 June 2015 are shown in Figure 7 along with various geomagnetic indices (SymH, AsyH, and AL) and interplanetary conditions (interplanetary magnetic field [IMF] Bz and SW dynamic pressure). It can be clearly observed that the longitudinal gradients have opposite signs during daytime and nighttime. During this storm period, the location of satellite C was always east of satellite A, and therefore, satellite C is ahead in longitude compared to satellite A. As satellite C is ahead in longitude, the denominator in equation (1) is a negative value $((\phi_{\mathrm{Sat\ A}}(\theta) - \phi_{\mathrm{Sat\ C}}(\theta)) \sim -1.45^{\circ})$. It should also be noted that the situation of crossing of zero longitude has been handled appropriately to fit in the negative denominator condition. The gradients in the day sector mostly show negative values in the main and early recovery phase. Whereas, the gradients in the night sector have mainly positive values.

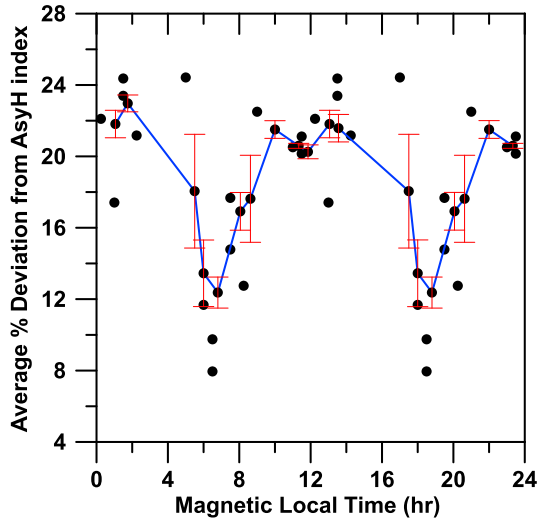

Figure 6. Average % deviation of asymmetry from AsyH index estimated in different magnetic local time sectors. The blue line shows the average pattern along with the standard error bars.

Now the question is what could be the source for the observed differences at satellites A and C? The gradients in the magnetospheric ring current or ionospheric currents could result in the differences at satellites A and C measurements. At low to equatorial latitudes, during daytimes, longitudinal gradients in the equatorial electrojet and Sq currents can produce the differences in the magnetic field observations; however, it would be very small within the longitudinal separation of ~1.5°. Also, at nighttimes *E* region ionospheric currents do not exist due to ceasing of ionospheric conductivity. Therefore, the observed gradients cannot be explained using ionospheric currents of equatorial electrojet and Sq. Considering a very small temporal separation between satellites A and C, the possibility of the temporal variations of ring current is also ruled out. Moreover, in case of the temporal variations, the gradients would have opposite signs in the main (descending variation) and recovery (ascending variation) phases, irrespective of daytime and nighttime, and hence, the gradients at day and night should have the same sign, which is not observed. Therefore, the gradients in the magnetospheric ring current could be the possible source for the observed longitudinal gradients.

During 2015, the longitudinal position of satellite C was east of satellite A. In order to visualize the situation, in Figure 8 we have sketched the

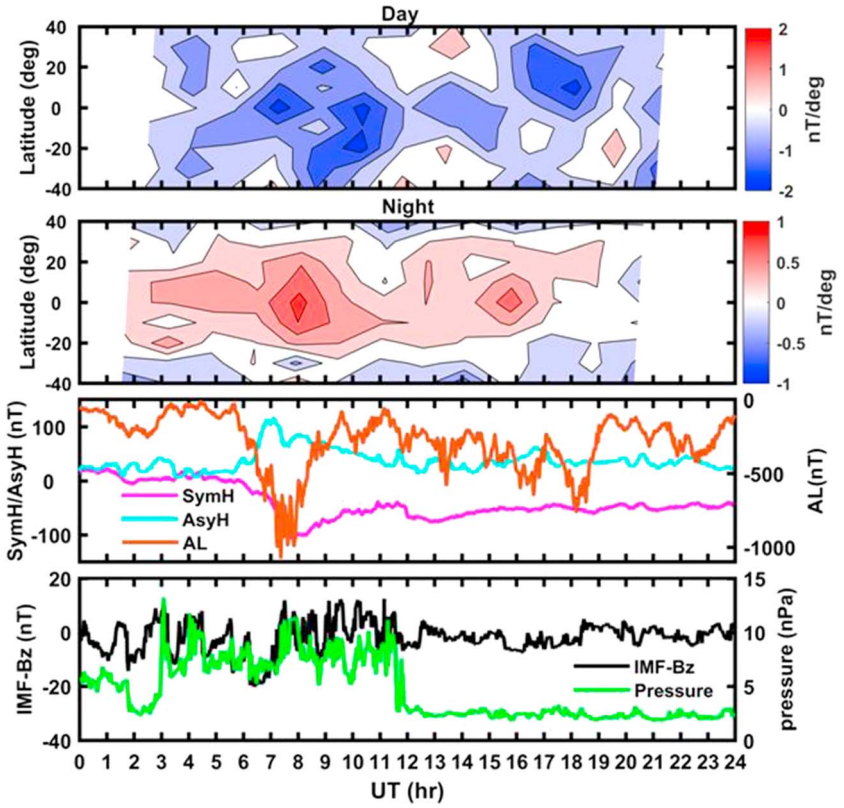

Figure 7. Geomagnetic storm on 8 June 2015: First two panels on the top indicate the contours of longitudinal gradients of storm time magnetic field variations plotted in the latitude-time frame, on the dayside and nightside. AL, SymH, and AsyH indices are shown in the second panel from bottom. The vertical components of the interplanetary magnetic field and solar wind dynamic pressure are shown in the bottom-most panel.

relative positions of satellites A and C in the equatorial plane in different LT sectors during 2015. In case of the injection of particles in the ring current from magnetotail, in the postmidnight to morning hours through dawn, the ring current at satellite A would be stronger than that at satellite C (as satellite A is more toward night). This would result in the stronger negative magnetic field variations at satellite A than that at satellite C, making the difference in the residual magnetic field (numerator of equation (1)) to be negative. Since denominator is also a negative quantity (location of satellite C is east of satellite A), the calculated gradients would have positive sign, On the other hand, between premidnight to postnoon sector through dusk, Sat C would experience stronger ring current than satellite A, making the magnetic field difference to be positive and hence negative gradient values. On 8 June 2015, the LT during day and night passes of satellites A and C at middle to low latitudes lied in the afternoon and postmidnight sectors (1215 and 0015). Thus, the gradients depicted in Figure 7 fit well into the scenario of particle injection from the magnetotail, with positive gradients in the postmidnight sector and negative gradient values in the post noon sector. These gradients are in general centered near the equator, showing similar pattern up to around 20–30° latitudes in the northern and southern hemispheres. Distinct peaks in the gradients are evident at ~8 and 16 UT, which could be associated with enhanced convection electric field due to southward turning of the IMF Bz. Thus, the gradient values estimated through present analysis support nighttime injection of the ring current particles during the main and early recovery phases.

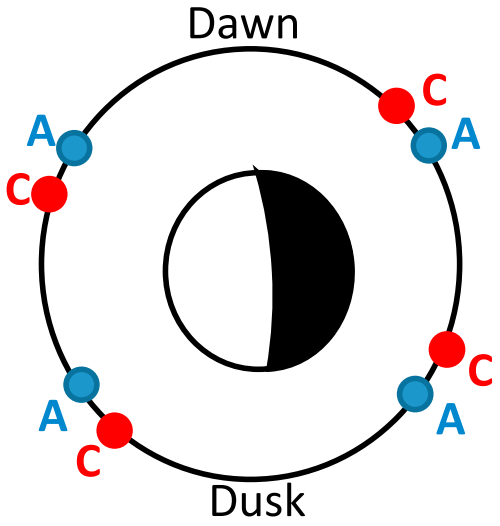

Figure 8. Sketch of relative positions of satellites A and C in the equatorial plane in different LT sectors, during 2015.

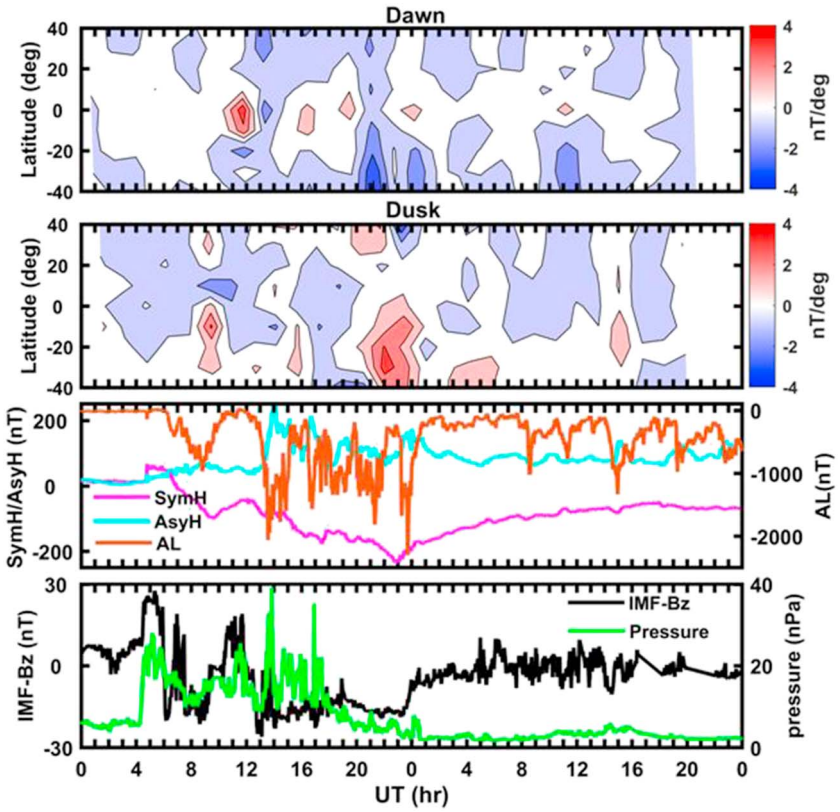

Figure 9. Same as Figure 7 but for 17–18 March 2015 geomagnetic storm.

In Figure 9, we present the gradient contours for another storm occurred on 17 March 2015 (traversing in the dawn and dusk sectors). As noticed before, there are multiple steps (depressions) during the main phase of this storm (SymH index). The gradient contours also exhibit little complex structures, unlike the previous case displayed in Figure 7. In general, the gradients show positive (negative) gradients in the dawn (dusk) sectors, at low latitudes, which is in accordance with the nighttime particle injection model of the ring current. In the dawn (dusk) zone, satellite A (being west of satellite C) would be more toward (away from) midnight, resulting in the positive (negative) values of the gradients near dawn (dusk). However, there are a few intervals when the above-mentioned trend reversed, for example, between 20 and 24 UT on 17 March. Also, during this time interval, stronger gradients are evident near higher latitudes ~30–40°, instead of near the equator. This may indicate the presence of additional current systems. One can notice the occurrence of substorm at ~23 UT on 17 March, which can result in intense sheet-like FACs (Iijima & Potemra, 1978), dissipating magnetospheric energy into the ionosphere (Akasofu, 1977). However, there were multiple substorms in the interval between 13 and 20 UT, during which gradients did not peak significantly at higher latitudes. One possible explanation for this observation could be that the location of the ring current moves earthward with the development of the ring current and also the equatorward boundary of the auroral oval shifts to the lower latitudes. This may result in the situation, where the field lines carrying the FACs would cross the LEO orbit at lower latitudes (~ ±40°). And hence LEO satellite would observe the gradients more effectively, compared to those when ring current is located away from the Earth. The recovery of the storm began at 23 UT on 17 March, and coincidently, there was an onset of a substorm, although IMF Bz turned northward only after 23 UT. Ohtani et al. (2001) have reported that if the beginning of the recovery phase observed in the SymH index coincides with the onset of the substorm, then it is not actual recovery of the ring current but the disruption of the tail current, which results in the reduced westward current and hence may appear as a recovery of the ring current.

6. Discussion

The residual magnetic field variations obtained after subtracting internal geomagnetic field and quiet time current contributions from the magnetic field recorded by Swarm spacecraft during magnetically active times contain the contributions mostly due to storm time currents. The residual fields obtained in this manner are found to follow the temporal profile of Dst variations very closely, during geomagnetic storms. To estimate the Dst values, we have utilized the residual fields at the equatorial crossings recorded by multiple spacecrafts traversing in different local time sectors. This is analogous to the traditional method of computation of Dst index from ground observatories located in different local times. However, the ground observatories are selected from the low to middle latitudinal belt, excluding near equatorial locations, to avoid the complications due to equatorial electrojet currents. And then estimating the ring current index at the equator (dividing by an average of the cosine of dipole latitude; Iyemori et al., Web publication wdc.kugi.kyoto-u.ac.jp, 2010). The present method utilizes directly the magnetic fields recorded at the equator and found to match very well with the ground-based Dst values. Out of three satellites of Swarm mission, two satellites (A and B) were separated by more than 20°, after April 2014. In this paper, we estimate Dst for the geomagnetic storms occurred between April 2014 and August 2015. It is found that the match between our estimates and ground-based Dst index is very good. The average deviation between these two is around 4–13%. In fact, sometimes the satellite-based Dst estimates match better with SymH index rather than ground-based Dst index. Thus, present analysis suggests that the conventional condition on the selection of ground-based observatories can be relaxed to include even near equatorial stations, while estimating Dst/SymH index.

We have noticed large differences between day/dawn and night/dusk magnetic field variations (Figure 3), particularly when AsyH index gets enhanced. Therefore, instead of opting for the traditional method for estimating asymmetry of the ring current (AsyH index), we have estimated the asymmetry by taking the difference between the residual magnetic field strengths at two MLT sectors separated by 12 hr. Our estimates show a good match with the AsyH index, especially when satellite traverses in the dawn-dusk sector. This indicates that the major source of asymmetry in the storm time current observed through ground measurements lies in the dawn-dusk sector.

We have noted that the variations are stronger in the dusk-to-night sectors compared to dawn-to-day sectors, in general. Our observation of higher magnetic field variations near dusk than dawn is consistent with the previous LEO satellite-based observations of storm time global Birkeland currents (Anderson et al., 2005). Using geomagnetic data from 98 low latitude to midlatitude stations, SuperMAG computes partial ring current indices at different local times (SMR-00, SMR-06, SMR-12, and SMR-18), which are available at http://supermag.jhuapl.edu/indices. Newell and Gjerloev (2012)) have reported that the SMR at different LTs differ significantly during geomagnetic storms, with larger amplitudes at dusk times. However, the statistical study using the curlometer technique on Cluster data revealed that the westward quiet time ring current (Dst > -30 nT) grows away from noon to dawnside and decays from midnight to noon through dusk region (Zhang et al., 2011). Thus, the observations at ground and LEO satellite heights differ from those at Cluster (~4–4.5 R_E altitude). Unlike magnetospheric missions, the altitude of observations using LEO spacecraft measurements is almost constant. Thus, the spatial and temporal scales of sampling differ significantly in the magnetospheric and near-Earth regions. Cluster results were explained by Zhang et al. (2011) through R2 FACs connecting magnetosphere and ionosphere. If the ring currents are fed by the upcoming R2 FACs at dawn and removed by the downward R2 currents near dusk, then it would give higher values near dawn than that at dusk. They also mention the other possibility that part of the enhanced current in certain MLT sectors could be due to an increase in the mean AE activity. The MLT pattern reported by Zhang et al. (2011) is basically for the quiet time ring current (Dst > -30 nT), while the study carried out in the present paperis explicitly during geomagnetic storms. We also notice that the difference between dawn and dusk values is significantly less during prestorm intervals. Therefore, it may not be appropriate to compare our results with Zhang et al. (2011). Using multispacecraft magnetic field observations by Cluster, Shen et al. (2014) found that the radius of curvature of the magnetic field lines reduces at all local times during geomagnetic storms, which changes ring current magnetic geometry and hence the spatial distribution of the particles with various energies in the plasmasphere, ring current, and radiation belts considerably. They further reported that during similar storm activity the radius of curvature of the local magnetic field lines is smallest on the nightside to duskside, medium on the dawnside, and largest on the dayside, suggesting large local time asymmetry.

Now the question is why the disturbed time magnetic fields presented in this paper have stronger values in night/dusk than day/dawn sectors? It is known that the pressure gradient currents $\left(\frac{\boldsymbol{B}}{B^2}\times\nabla\boldsymbol{P}_{\perp}\right)$ form an important contribution to the azimuthally circulating ring current around the Earth (Lui et al., 1987; Vasyliunas, 1984). If the pressure gradients at the outer boundary are uniform in all LT sectors, then the ring current would be symmetric in all LTs. The differences in the storm time current at dawn and dusk sector may suggest an unequal plasma pressure gradient at dawn and dusk. Interestingly, Lui (2003) observed that the proton pressure is generally higher in the dusk midnight sector than in the postmidnight sector during high Kp values. The higher plasma pressures at dusk can be explained as follows: The movement of ions from nightside to dusk may result in larger plasma densities at dusk than that at dawn, due to possibilities of scattering of charged particles before they reach dawn. Also, the ion temperatures are higher than the electron temperatures. Therefore, the plasma pressure ($P = nkT$) in the ring current is higher at dusk, and consequently, the pressure gradients with respect to the outer magnetosphere are also high. This would eventually produce larger ring currents at dusk. The additional contribution from the magnetotail currents could be responsible for the larger values in the nighttime sectors (Kalegaev et al., 2005).

Since the longitudinal and latitudinal separation between the orbits of satellites A and C is very small, it is possible to gain knowledge about the longitudinal gradients in the storm time currents and their latitudinal extent. Use of the other pair of satellites A/C and B to compute the longitudinal gradients is not possible as the latitudinal difference between satellites A/C and B is very high, which can introduce very large temporal variations in the computations of gradients. For example, during 8 June 2015 event, the latitudinal difference between satellites A and B can be as large as 145°, giving time difference of ~36 min. This indicates that satellites A and B may fall in different LT sectors. So other than temporal variations, gradients due to difference in LT sectors also get introduced. At the same time, large latitudinal differences can also introduce gradients due to different current sources acting at different latitudes. Therefore, computing gradients using A/C and B will not be helpful in drawing a meaningful conclusion. Also, it is important to note that the satellite B orbiting at a higher altitude has different orbital velocity compared to that of satellites A and C. Therefore, the latitudinal difference of satellite B from satellite A/C is not constant. It changes from pass to pass. Thus, the value of the latitudinal difference mentioned above is true for a particular pass, and it changes during the consecutive passes. On the other hand, satellites A and C maintain the same speed after orbital maneuvering period (after April 2014). So they maintain a constant latitudinal distance, which is around 0.5° after April 2014, and hence, temporal variations of ~ 7 s are very small. Therefore, the gradients calculated using satellites A and C is an appropriate pair for the computation of gradients, rather than satellites A/C and B.

It is observed that in general, the gradients are stronger near the equator during the main phase of the storm with a latitudinal width of ~20–30° in each hemisphere. Significant gradient values observed during nighttimes near equator rule out the contribution due to gradients in the ionospheric currents such as equatorial electrojet. The gradients in the postmidnight to prenoon sector and in the postnoon to premidnight sector have opposite signs. This eliminates the possibility of the contribution due to temporal variations of the ring current, in the observed longitudinal gradients. The observed feature of exactly opposite gradients in the opposite local time sectors is found to be consistent with the scenario of particle injection from the magnetotail (explained in section 5). The stronger gradients are observed at higher latitudes during the episodes of substorms, which might be associated with the ionospheric currents related to FACs.

7. Summary

1. The present paper studies the magnetic field measurements recorded by multisatellite polar orbiting mission, Swarm, during magnetically active times.
2. During geomagnetic storm period, the residual magnetic field can be considered as a proxy for storm time currents and are found to follow the temporal profile of Dst/SymH variations very closely.
3. These variations at the equatorial crossings recorded by multiple spacecraft are used to estimate the Dst values and are found to have a good match with the ground-based Dst index. The average deviation between these two is around 4–13%. Therefore, the present study suggests that the accustomed condition on the selection of ground observatories to estimate Dst/SymH indices can be relaxed to include even near equatorial stations.

4. We have estimated the asymmetry in storm time currents by taking the difference between the magnetic field variations at two local time sectors separated by 12 hr, which shows a good match with the AsyH index, especially when satellite traverses in the dawn-dusk sector. This indicates that the dominant source of asymmetry in the ring current observed through AsyH index lies in the dawn-dusk sector.
5. In general, the magnetic field variations are stronger in the dusk-to-night sector than dawn-to-day sector, which could be due to the larger pressure-gradients near night-to-dusk caused by the ion movements.
6. The important advantage of Swarm mission is that it provides an opportunity to investigate the longitudinal gradients in the ring current.
7. The azimuthal gradients in the postmidnight to prenoon sector and in the postnoon to premidnight sector have opposite signs.
8. It is observed that in general, the gradients are stronger near the equator during the main phase of the storm with a latitudinal width of ~20–30° in each hemisphere and are supportive to the idea of particle-injection from the magnetotail.
9. The stronger gradients are observed at higher-latitudes (~40°) during the episodes of substorms and might be associated with the ionospheric/FACs.

Acknowledgments
The European Space Agency (ESA) is acknowledged for providing high-quality magnetic field data from Swarm satellites. The Swarm data used here is MAGX_LR_1B and is freely accessible at http://earth.esa.int/web/guest/swarm/data-access. We also thank WDC for Geomagnetism, Kyoto (http://wdc.kugi.kyotou.ac.jp/caplot/index.html), for providing various indices used in the study. This work is supported by the Department of Science and Technology, Government of India. The work is partly supported by ISEE International Collaborative Research Program, and JSPS KAKENHI (15H05815 and 16H06286). A. B. acknowledges the support by the NASA Living With a Star Jack Eddy Postdoctoral Fellowship Program, administered by UCARs CPAESS.

References

Abdu, M. A., de Souza, J. R., Sobral, J. H. A., & Batista, I. S. (2006). Magnetic storm associates disturbance dynamo effects over low and equatorial latitude ionosphere. In B. Tsurutani et al. (Eds.), *Recurrent magnetic storms: Corotating solar wind streams*, *Geophysical Monograph Series* (Vol. 167, pp. 283–304). Washington, DC: American Geophysical Union. https://doi.org/10.1029/167GM22

Akasofu, S.-I. (1977). *Physics of magnetospheric substorms* (pp. 473–474). Hingham, Mass: D. Reidel.

Akasofu, S. I., & Chapman, S. (1964). On the asymmetric development of magnetic storm fields in low and middle latitudes. *Planetary and Space Science*, *12*(6), 607–626. https://doi.org/10.1016/0032-0633(64)90008-X

Anderson, B. J., Ohtani, S.-I., Korth, H., & Ukhorskiy, A. (2005). Storm time dawn-dusk asymmetry of the large-scale Birkeland currents. *Journal of Geophysical Research*, *110*, A12220. https://doi.org/10.1029/2005JA011246

Astafyeva, E., Zakharenkova, I., & Alken, P. (2016). Prompt penetration electric fields and the extreme topside ionospheric response to the June 22–23, 2015 geomagnetic storm as seen by the Swarm constellation. *Earth, Planets and Space*, *68*, 152. https://doi.org/10.1186/s40623-016-0526-x

Balan, N., Liu, J. Y., Otsuak, Y., Tulasi Ram, S., & Luhr, H. (2012). Ionospheric and thermospheric storms at equatorial latitudes observed by CHAMP, ROCSAT and DMSP. *Journal of Geophysical Research*, *117*, A01313. https://doi.org/10.1029/2011JA016903

Balasis, G., Daglis, I. A., Zesta, E., Papadimitriou, C., Georgiou, M., Haagmans, R., & Tsinganos, K. (2012). ULF wave activity during the 2003 Halloween superstorm: Multipoint observations from CHAMP, Cluster and Geotail missions. *Annales de Geophysique*, *30*(12), 1751–1768. https://doi.org/10.5194/angeo-30-1751-2012

Brandt, P. C.:s., Mitchell, D. G., Ebihara, Y., Sandel, B. R., Roelof, E. C., Burch, J. L., & Demajistre, R. (2002). Global IMAGE/HENA observations of the ring current: Examples of rapid response to IMF and ring current-plasmasphere interaction. *Journal of Geophysical Research*, *107*(A11), 1359. https://doi.org/10.1029/2001JA000084

Daglis, I., Thorne, R. M., Baumjohann, W., & Orsini, S. (1999). The terrestrial ring current: Origin, formation, and decay. *Reviews of Geophysics*, *37*(4), 407–438. https://doi.org/10.1029/1999RG900009

De Michelis, P., Consolini, G., Tozzi, R., & Marcucci, M. F. (2016). Observations of high-latitude geomagnetic field fluctuations during St. Patrick's Day storm: Swarm and SuperDARN measurements. *Earth, Planets and Space*, *68*, 105. https://doi.org/10.1186/s40623-016-0476-3

Dubyagin, S., Ganushkina, N., Kubyshkina, M., & Liemohn, M. (2014). Contribution from different current systems to *SYM* and *ASY* midlatitude indices. *Journal of Geophysical Research: Space Physics*, *119*, 7243–7263. https://doi.org/10.1002/2014JA020122

Dungey, J. W. (1961). Interplanetary magnetic field and the auroral zones. *Physical Review Letters*, *6*(2), 47–48. https://doi.org/10.1103/PhysRevLett.6.47

Dunlop, M. W., Balogh, A., Glassmeier, K.-H., & Robert, P. (2002). Four-point Cluster application of magnetic field analysis tools: The curlometer. *Journal of Geophysical Research*, *107*(A11), 1384. https://doi.org/10.1029/2001JA005088

Dunlop, M. W., Southwood, D. J., Glassmeier, K.-H., & Neubauer, F. M. (1988). Analysis of multipoint magnetometer data. *Advances in Space Research*, *8*(9-10), 273–277. https://doi.org/10.1016/0273-1177(88)90141-X

Dunlop, M. W., Yang, J. Y., Yang, Y. Y., Xiong, C., Lühr, H., Bogdanova, Y. V., et al. (2015). Simultaneous field-aligned currents at Swarm and Cluster satellites. *Geophysical Research Letters*, *42*, 3683–3691. https://doi.org/10.1002/2015GL063738

Friedrich, E., Rostoker, G., & Connors, M. G. (1999). Influence of the substorm current wedge on the Dst index. *Journal of Geophysical Research*, *104*(A3), 4567–4575. https://doi.org/10.1029/1998JA900096

Friis-Christensen, E., Luhr, H., & Hulot, G. (2006). *Swarm*: A constellation to study the Earth's magnetic field. *Earth, Planets and Space*, *58*, 351. https://doi.org/10.1186/BF03351933

Greenspan, M. E., & Hamilton, D. C. (2000). A test of the Dessler- Parker-Sckopke relation during magnetic storms. *Journal of Geophysical Research*, *105*(A3), 5419–5430. https://doi.org/10.1029/1999JA000284

Hamilton, B. (2013). Rapid modelling of the large-scale magnetospheric field from Swarm satellite data. *Earth, Planets and Space*, *65*(11), 1295–1308. https://doi.org/10.5047/eps.2013.09.003

Horvath, I., & Lovell, B. C. (2014). Perturbation electric fields and disturbance currents investigated during the 25 September 1998 great storm. *Journal of Geophysical Research: Space Physics*, *119*, 8483–8498. https://doi.org/10.1002/2014JA020480

Iijima, T., & Potemra, T. A. (1978). Large-scale characteristics of field-aligned currents associated with substorms. *Journal of Geophysical Research*, *83*(A2), 599–615. https://doi.org/10.1029/JA083iA02p00599

Jadhav, G., Rajaram, M., & Rajaram, R. (2002a). A detailed study of equatorial electrojet phenomenon using Ørsted satellite observations. *Journal of Geophysical Research*, *107*(A8), SIA 12-1–SIA 12-12. https://doi.org/10.1029/2001JA000183

Jadhav, G., Rajaram, M., & Rajaram, R. (2002b). Main field control of the equatorial electrojet: A preliminary study from the Ørsted data. *Journal of Geodynamics*, *33*(1–2), 157–171. https://doi.org/10.1016/S0264-3707(01)00061-8

Kalegaev, V. V., Ganushkina, N. Y., Pulkinen, T. I., Kubyshkina, M. V., Singer, H. J., & Russell, C. T. (2005). Relation between the ring current and the tail current during magnetic storms. *Annales de Geophysique*, *23*(2), 523–533. https://doi.org/10.5194/angeo-23-523-2005

Kamide, Y., McPherron, R. L., Gonzalez, W. D., Hamilton, D. C., Hudson, H. S., Joselyn, J. A., et al. (1997). Magnetic storms: Current understanding and outstanding questions. In B. T. Tsurutani et al. (Eds.), *Magnetic storms* (pp. 1–19). Washington, DC: American Geophysical Union. https://doi.org/10.1029/GM098p0001

Lanzerotti, L. J., & Gerrard, A. J. (2016). Ring current ions measured by the RBSPICE instrument on the Van Allen Probes mission. In C. R. Chappell et al. (Eds.), *Magnetosphere-Ionosphere Coupling in the Solar System*, *American Geophysical Union Geophysical Monograph Series* (Chap. 1). Hoboken, NJ: John Wiley.

Liemohn, M. W., Kozyra, J. U., Thomsen, M. F., Roeder, J. L., Lu, G., Borovsky, J. E., & Cayton, T. E. (2001). Dominant role of the asymmetric ring current in producing the stormtime Dst. *Journal of Geophysical Research*, *106*(A6), 10,883–10,904. https://doi.org/10.1029/2000JA000326

Lühr, H., Park, J., Gjerloev, J. W., Rauberg, J., Michaelis, I., Merayo, J. M. G., & Brauer, P. (2015). Field-aligned currents' scale analysis performed with the Swarm constellation. *Geophysical Research Letters*, *42*, 1–8. https://doi.org/10.1002/2014GL062453

Lühr, H., Warnecke, J., Zanetti, L., Lindqvist, P. A., & Hughes, T. J. (1994). Fine structure of field-aligned current sheets deduced from spacecraft and ground-based observations: Initial Freja results. *Geophysical Research Letters*, *21*, 1883–1886. https://doi.org/10.1029/94GL01278

Lui, A. T. Y. (2003). Inner magnetospheric plasma pressure distribution and its local time asymmetry. *Geophysical Research Letters*, *30*(16), 1846. https://doi.org/10.1029/2003GL017596

Lui, A. T. Y., McEntire, R. W., & Krimigis, S. M. (1987). Evolution of the ring current during two geomagnetic storms. *Journal of Geophysical Research*, *92*(A7), 7459–7470. https://doi.org/10.1029/JA092iA07p07459

Manoj, C., Maus, S., & Alken, P. (2013). Long-period prompt-penetration electric fields derived from CHAMP satellite magnetic measurements. *Journal of Geophysical Research: Space Physics*, *118*, 5919–5930. https://doi.org/10.1002/jgra.50511

Munsami, V. (2000). Determination of the effects of substorms on the storm-time ring current using neural networks. *Journal of Geophysical Research*, *105*(A12), 27,833–27,840. https://doi.org/10.1029/2000JA000041

Newell, P. T., & Gjerloev, J. W. (2012). SuperMAG-based partial ring current indices. *Journal of Geophysical Research*, *117*, A05215. https://doi.org/10.1029/2012JA017586

Ohtani, S., Nosé, M., Rostoker, G., Singer, H., Lui, A. T. Y., & Nakamura, M. (2001). Storm substorm relationship: Contribution of the tail current to Dst. *Journal of Geophysical Research*, *106*(A10), 21,199–21,209. https://doi.org/10.1029/2000JA000400

Oliveira, D. M., Zesta, E., Schuck, P. W., & Sutton, E. K. (2017). Thermosphere global time response to geomagnetic storms caused by coronal mass ejections. *Journal of Geophysical Research: Space Physics*, *122*, 10,762–10,782. https://doi.org/10.1002/2017JA024006

Olsen, N., Finlay, C. C., Kotsiaros, S., & Tøffner Clausen, L. (2016). A model of Earth's magnetic field derived from two years of Swarm data. *Earth, Planets and Space*, *68*(1). https://doi.org/10.1186/s40623-016-0488-z

Olsen, N., Friis-Christensen, E., Floberghagen, R., Alken, P., Beggan, C. D., Chulliat, A., et al. (2013). The *Swarm* Satellite Constellation Application and Research Facility (SCARF) and *Swarm* data products. *Earth, Planets and Space*, *65*, 1. https://doi.org/10.5047/eps.2013.07.001

Olsen, N., Lühr, H., Finlay, C. C., & Tøffner-Clausen, L. (2014). The CHAOS-4 geomagnetic field model. *Geophysical Journal International*, *1997*, 815–827.

Rangarajan, G. K. (1989). Indices of geomagnetic activity. In J. A. Jacobs (Ed.), *Geomagnetism* (Vol. 2, pp. 323–384). London, UK: Academic Press.

Robert, P., Dunlop, M. W., Roux, A., & Chanteur, G. (1998). Accuracy of current density determination, in analysis methods for multi-spacecraft data, ISSI Sci. Rep., SR-001, Kluwer Acad, Noordwijk, Netherlands.

Shen, C., Yang, Y. Y., Rong, Z. J., Li, X., Dunlop, M., Carr, C. M., et al. (2014). Direct calculation of the ring current distribution andmagnetic structure seen by Cluster during geomagnetic storms. *Journal of Geophysical Research: Space Physics*, *119*, 2458–2465. https://doi.org/10.1002/2013JA019460

Siscoe, G. L., & Crooker, N. U. (1974). On the ring current contribution to Dst. *Journal of Geophysical Research*, *79*(7), 1110–1112. https://doi.org/10.1029/JA079i007p01110

Sugiura, M. (1964). Hourly values of the equatorial Dst for IGY. In *Annals of the International Geophysical Year* (Vol. 35, pp. 945–948). Oxford, UK: Pergamon.

Thomas, N., Vichare, G., & Sinha, A. K. (2017). Characteristics of equatorial electrojet derived from Swarm satellites. *Advances in Space Research*, *59*(6), 1526–1538. https://doi.org/10.1016/j.asr.2016.12.019

Turner, N. E., Baker, D. N., Pulkkinen, T. I., & McPherron, R. L. (2000). Evaluation of the tail current contribution to Dst. *Journal of Geophysical Research*, *105*(A3), 5431–5439. https://doi.org/10.1029/1999JA000248

Vasyliunas, V. M. (1984). Fundamentals of current description. In T. A. Potemra (Ed.), *Magnetospheric currents*, *Geophysical Monograph Series* (Vol. 28, pp. 63–66). Washington, DC: American Geophysical Union.

Vichare, G., & Rajaram, R. (2011). Global features of quiet time counterelectrojet observed by Ørsted. *Journal of Geophysical Research*, *116*, A04306. https://doi.org/10.1029/2009JA015244

Weygand, J. M., & McPherron, R. L. (2006). Dependence of ring current asymmetry on storm phase. *Journal of Geophysical Research*, *111*, A11221. https://doi.org/10.1029/2006JA011808

Zhang, Q.-H., Dunlop, M. W., Lockwood, M., Holme, R., Kamide, Y., Baumjohann, W., et al. (2011). The distribution of the ring current: Cluster observations. *Annales de Geophysique*, *29*(9), 1655–1662. https://doi.org/10.5194/angeo-29-1655-2011